Materials Science & Engineering A 573 (2013) 141–147

Contents lists available at SciVerse ScienceDirect

Materials Science & Engineering A

journal homepage: www.elsevier.com/locate/msea

Strength scaling law, deformation kinetics and mechanisms of nanostructured Ti

Y.K. Li [a,b], F. Liu [a], G.P. Zheng [b], D. Pan [a], Y.H. Zhao [c], Y.M. Wang [d,*]

[a] School of Materials Science and Engineering, The University of Shanghai for Science and Technology, Shanghai, China
[b] Department of Mechanical Engineering, The Hong Kong Polytechnic University, Hung Hom, Kowloon, Hong Kong
[c] School of Materials Science and Engineering, Nanjing University for Science and Technology, Nanjing, Jiansu, China
[d] Physical and Life Sciences Directorate, Lawrence Livermore National Laboratory, Livermore, CA, USA

ARTICLE INFO

Article history:
Received 24 December 2012
Received in revised form
21 February 2013
Accepted 25 February 2013
Available online 6 March 2013

Keywords:
Nanostructured Ti
Strain rate sensitivity
Activation volume
Hall–petch relationship
Internal friction

ABSTRACT

We investigate the tensile properties, strain rate sensitivity, and activation volume of nanostructured Ti prepared by equal channel angular pressing plus a series of thermal treatment. Simultaneous enhancement of strength and tensile ductility is achieved. The strain rate sensitivity is found to decrease with decreasing grain sizes (~150–450 nm). A new Hall–petch relationship is presented and discussed. The analyses on the internal friction peaks at around −70 °C suggest that twins could play the primary role for the strain hardening of the annealed nanostructured Ti, consistent with the miniscule activation volumes.

1. Introduction

Due to its excellent mechanical properties, light weight, good corrosion resistance, and biocompatibility, ultrafine-grained (UFG) or nanocrystalline (NC) titanium (Ti) has attracted a great deal of attention over the last decade [1–3]. To date, the majority of UFG-Ti materials have been prepared by equal channel angular pressing (ECAP), which has the advantage of retaining the bulk dimensions. Despite the coveted strength (< 900 MPa), however, the ECAP-Ti is known to suffer from early necking instability and hardly owns much useful tensile ductility [4]. Hence, post-ECAP processing such as thermomechanical treatment is often necessary in order to recover uniform tensile ductility for advanced structural applications. Simultaneous enhancement in both strength and ductility have indeed been achieved through short-time annealing [5,6], the origin of which was attributed to the grain boundary (GB) structures. However, reproducible production of such materials has not been forthcoming due to the degree of difficulty in pinpointing heat treatment conditions and the potential impacts of other variables such as impurities on the GB structures.

On the other hand, the deformation mechanism in hexagonal-close-packed (HCP) nanostructured metals (e.g., Ti, Mg) is an intriguing problem that has not been completely resolved in the literature [7,8]. Some important deformation kinetics parameters such as strain rate sensitivity and activation volume, or even the classical Hall–petch scaling law, are not well-established for nanostructured Ti materials. Because of the complicated microstructure existing in ECAP samples (i.e., both twins and dislocations), it remains a challenge to elucidate the deformation mechanisms using postmortem microstructure characterizations [9]. In a recent study of Ti single crystal pillars [10], deformation twinning is found less important when the pillar size reduces below ~1 μm and the sample surface starts to play a significant role. Interestingly, an inversed size-dependent twinning phenomenon is observed in HCP NC cobalt [11], where GBs play an important role. These experimental investigations suggest that there is no unified picture on the deformation mechanisms especially twinning behavior in HCP materials when the grain size or sample dimension reaches submicron or nanometer regime [12]. Note that deformation twinning could play deterministic role in the tensile ductility of some HCP metals such as Mg alloys [8].

Through a series of thermal heat treatment, here we employ tensile tests and nanoindentation to systematically explore the achievable mechanical properties for nanostructured Ti prepared by ECAP. We investigate the deformation kinetics and strength scaling law for these materials. Simultaneous enhancement in both strength and ductility is achieved for samples annealed at low temperatures for several hours. Moreover, dynamic mechanical analyses (DMA) are applied to survey the underlying deformation

* Corresponding authors. Tel.: +1 925 4226082; fax: +1 925 4224664.
E-mail addresses: mmzheng@polyu.edu.hk (G.P. Zheng), ymwang@llnl.gov (Y.M. Wang).

0921-5093/$ - see front matter © 2013 Elsevier B.V. All rights reserved.
http://dx.doi.org/10.1016/j.msea.2013.02.054

mechanisms of ECAP- and annealed-Ti samples with UFG structures. Activation energy is calculated from DMA spectra and used to interpret the possible deformation mechanisms.

2. Experimental

Commercial purity (CP) Ti (ASTM grade 2) with a composition (wt%) of 0.34% O, 0.2% Fe, 0.05% C, 0.005% N, and balanced Ti was used as the starting material. The billets were subjected to ECAP processing with route B_C for 4 passes at room temperature, followed by annealing at 350–500 °C for different time intervals (0.5–6 h). Table 1 summarizes the sample conditions. The microstructure of all samples was examined using transmission electron microscopy (TEM, JEOL JEM-2100) along the longitudinal direction (i.e., parallel to the ECAP axis). TEM specimens were prepared by mechanical polishing to a thickness of ~80 μm and further thinned to electron transparency using a twin-jet polishing with a solution of 5% perchloric acid, 35% butanol and 60% methanol at a temperature of −40 °C and an applied voltage of 40 V. Bright- and dark-field TEM images were taken at an accelerating voltage of 200 kV. The gauge dimension of dogbone tensile samples is 10 mm (length) × 2 mm (width) × 1 mm (thickness). The tensile tests were performed at a strain rate of $1\times10^{-3}\,s^{-1}$ in the ambient environment. Nanoindentation tests were conducted at room temperature using nanoindenter G200 (Agilent Inc.) with a Berkovich diamond indenter. All the hardness measurements were conducted along the direction normal to the pressing axis. The strain rate sensitivity (m) was measured at loading rates ranging from 70 mN/s to 0.705 mN/s. At least nine tests were repeated at each loading rate. The strain rate sensitivity (m) and the activation volume (V) are calculated according to

$$m=\frac{\partial \ln H}{\partial \ln \dot{\varepsilon}}, \tag{1}$$

and

$$V=\frac{3\sqrt{3}kT}{mH}, \tag{2}$$

where H is the hardness, $\dot{\varepsilon}$ strain rate, k the Boltzmann constant, and T the absolute temperature. Internal friction and storage modulus of the samples as a function of temperature were measured in a dynamic mechanical analyzer (DMA Q800, TA

Table 1
A summary of Ti materials used in this study, and the measured mechanical properties. The Burgers vector $b=0.295$ nm (i.e., assuming the a-type dislocations).

Sample conditions	Average grain size (nm)	Hardness (GPa)	$\sigma_{0.2\%}$ (GPa)	Ratio ($H/\sigma_{0.2\%}$)	Strain rate sensitivity (m)	Activation volume
As-ECAP	168	3.71	0.763	4.86	0.013	$7b^3$
ECAP+350 °C 6 h	263	3.76	0.796	4.72	0.019	$12b^3$
ECAP+400 °C 0.5 h	251	2.91	0.657	4.43	0.022	$13b^3$
ECAP+500 °C 0.5 h	290	2.78	0.560	4.96	0.0305	$10b^3$
ECAP+500 °C 1 h	453	2.29	0.519	4.41	0.042	$9b^3$

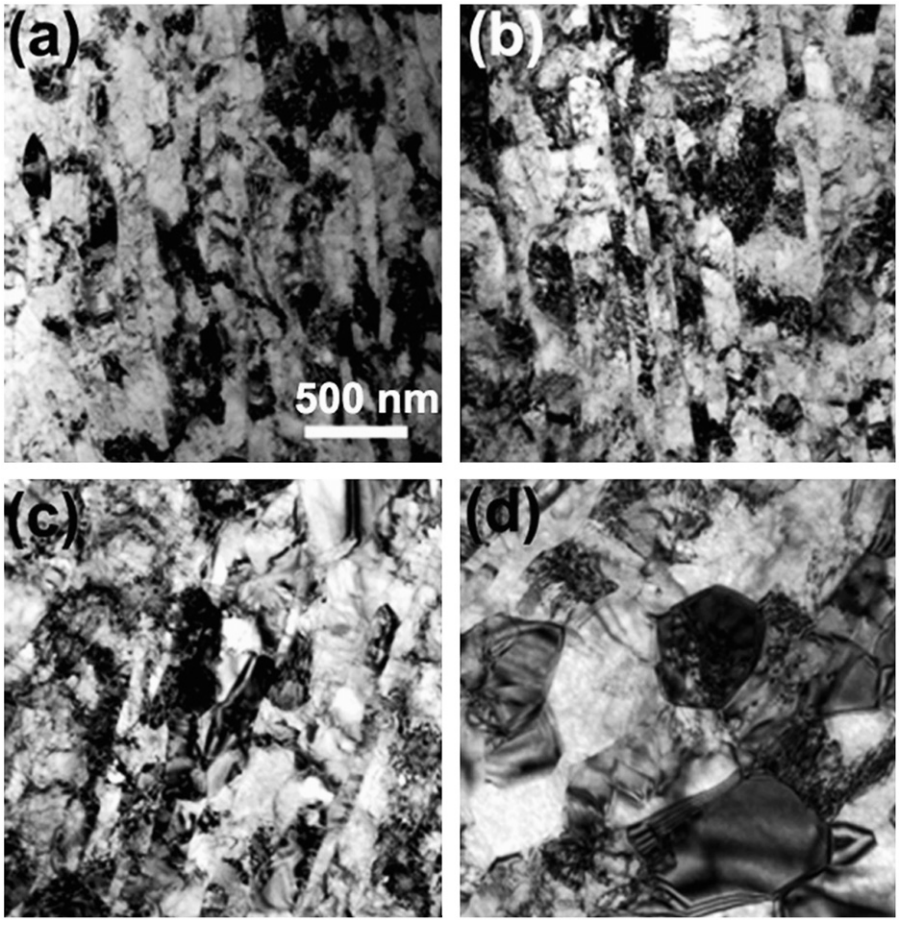

Fig. 1. Representative TEM images of Ti samples prepared by different processing conditions: (a) as-ECAP; (b) ECAP+400 °C for 0.5 h; (c) ECAP+500 °C for 0.5 h; and (d) ECAP+500 °C for 1 h. The scale bar for all images is 500 nm. The grain size distribution is measured along the grain width direction.

Instruments) from room temperature to −150 °C at different frequencies in a single-point bending mode. The cooling rate is 2 °C/min.

3. Results and discussions

3.1. Simultaneous high strength and high ductility

Fig. 1(a)–(d) display representative TEM micrographs of ECAP- and annealed-Ti samples, which indicate that the grain morphology evolves from highly-elongated structures to more equiaxed shapes as the annealing temperature increases. The grain coarsening is also evident, suggestive of recrystallization activities. Residual dislocations and twins remain observable but decrease with increased annealing temperatures and holding time. These results suggest that pre-existing deformation twins induced during the ECAP can be annealed away as the temperature arises (> 350 °C). To quantify the grain size (D) information, we manually measure D from a series of bright-field TEM images taken for each sample condition. The average D obtained from grain size histograms shown in Fig. 2 are compiled in Table 1. Note that the *D* of all samples is in the UFG regime, despite clear dislocation density difference.

The tensile engineering stress–strain curves of ECAP- and annealed-Ti samples shown in Fig. 3(a) indicate that post-ECAP heat treatment can produce samples with an impressive combination of tensile strength and tensile ductility. Interestingly, the sample annealed at 350 °C for 6 h exhibits simultaneous enhancement in both strength and ductility vis-à-vis those annealed at higher temperatures. The 0.2% yield strength ($\sigma_{0.2\%}$) of this sample is 0.796 GPa, with a total tensile elongation to failure of more than ~30%. Although annealing-induced enhancement in both strength

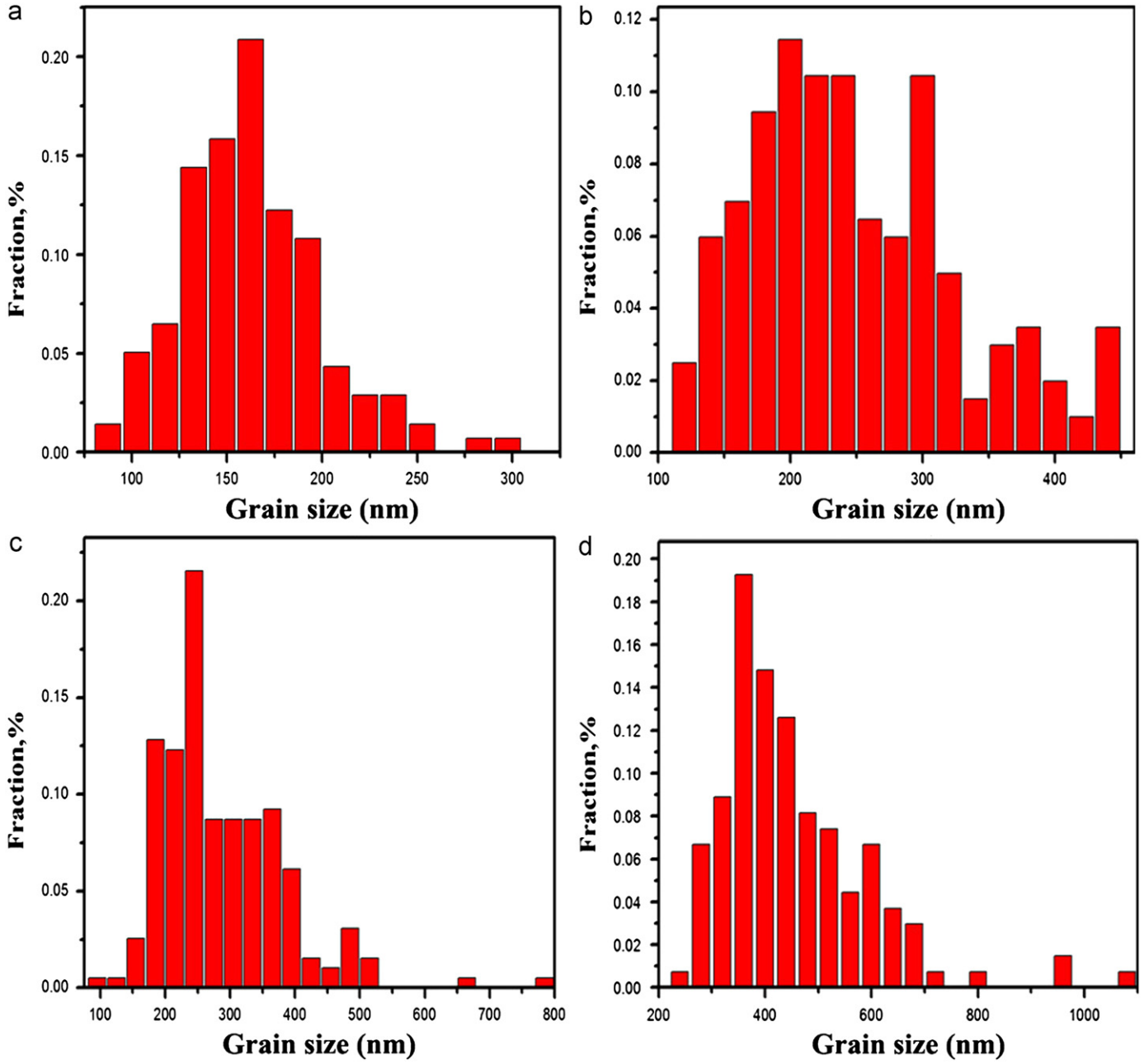

Fig. 2. Grain size distribution histograms for the four samples presented in Fig. 1. The order of the plots follows the exact same order of the TEM images; i.e., (a)–(d) are from samples of as-ECAP, ECAP+400 °C for 0.5 h, ECAP+500 °C for 0.5 h, ECAP+500 °C for 1 h, respectively.

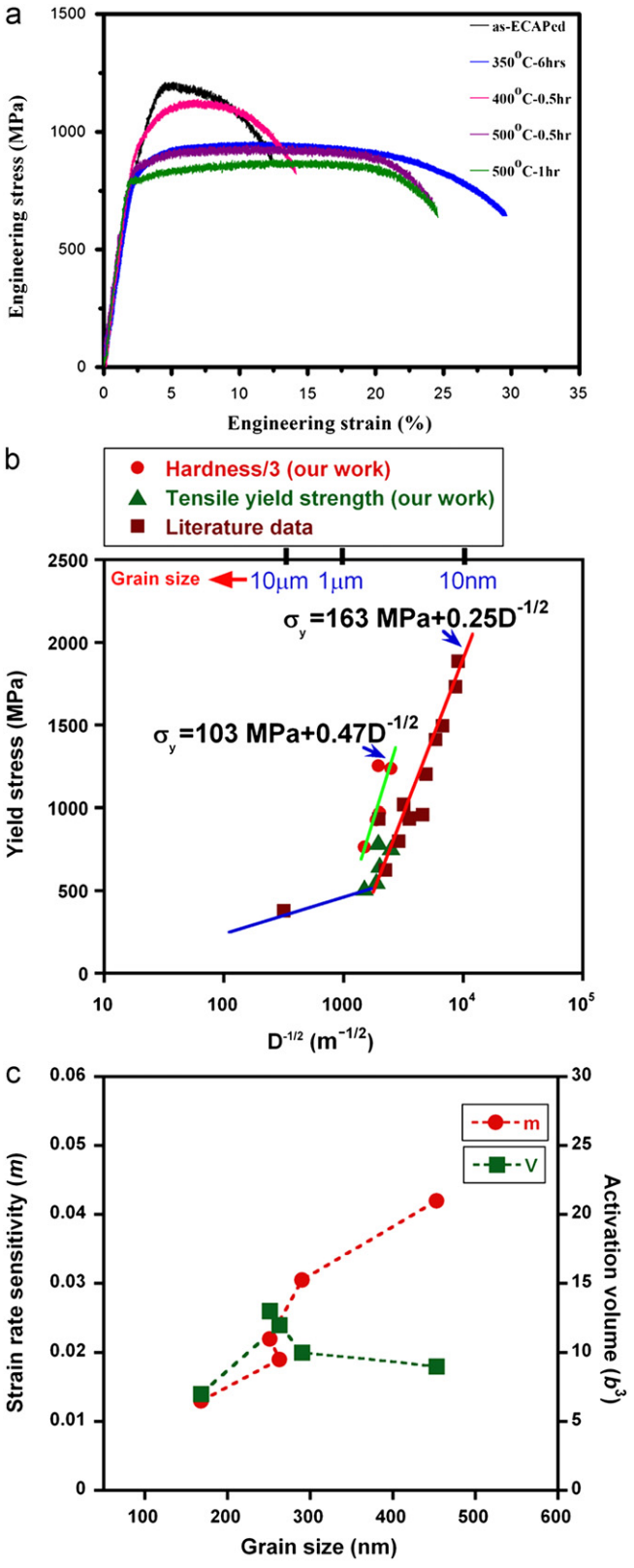

Fig. 3. (a) Tensile engineering stress-strain curves for various UFG-Ti samples. (b) A Hall–petch plot using the data report here and from the literature (references [6,18–22]). (c) Measured strain rate sensitivity (m) and activation volume (V) as a function of grain size (D) for UFG-Ti.

and ductility has been reported in several nanostructured metals [5,6,13–15], the origin of this behavior can be perversely complex. In the case of nanostructured Ti, the measured D in 350 °C treated sample is smaller or similar to other samples; however, the pre-existing deformation twins are preserved due to its low annealing temperature. In addition, grain interiors are relatively free of dislocations due to the long annealing hours. We thus speculate that the pre-existing twins may have played a critical role in achieving simultaneous high strength and high ductility. The ability of twin boundaries in helping retain high strength and high ductility has indeed been well-recognized in nanotwinned copper [16]. However, this phenomenon has seldom been studied in HCP materials due to their propensity to deformation twinning, which complicates the mechanistic studies. Interestingly, earlier studies have demonstrated that nanostructured Ti with multi-model distribution of grain sizes can also achieve both high strength and high ductility [17] (yield strength ~840 MPa, tensile elongation to failure ~27.5%), which is unlikely applicable to our case as we do not find bimodal or multi-modal grain structures in all of our samples (see Fig. 2). In contrast to some earlier experiments that typically use very short annealing time of a few minutes [6,13], we note that our experiments apply long annealing time (i.e., 6 h) in order to achieve both strength and ductility. Therefore, we believe that our approach is more controllable and could have more practical applications.

3.2. Hall–petch relationship for HCP Ti

To compare the hardness and strength measured in our samples with others, we investigate the Hall–petch (H–P) scaling law for our materials, Fig. 3(b), including the literature data from Refs. [6,18–22]. The tensile yield strength data measured from our samples seem to fit the literature data quite well; a linear-least-squares fit yields a H–P slope (K_y) of 0.25 MPa $m^{1/2}$, whereas the same linear fit using hardness-only data yields a substantially higher K_y=0.47 MPa $m^{1/2}$. Interesting, there apparently exist two H–P slopes in different grain size regions; i.e., microsized grain region and ultrafine- and nano-grain region. The origin of such behavior could be related to the grain size dependent twinning behavior in HCP materials but requires further investigations. Table 2 summarizes several H–P relationships reported from several other groups [21,23–27], as well as ours. The relative scattering of K_y in the literature for Ti can be attributed to the following reasons: (1) Materials purity. It is known that the strength of HCP metals is more sensitive to impurities than face-centered-cubic (FCC) metals, which contributes different K_y seen in the literature; (2) The contribution of dislocation/twin to the strength is often not considered; this is especially true when the ECAP samples were used for scaling law analysis; (3) The applicability of Tabor equation to HCP metals remain questionable. Our studies here reveal that the constant of proportionality (C) seen in our samples is mostly larger than four instead of the value of three (see Table 1). These results strongly suggest that the hardness measurements are likely to overestimate the K_y

Table 2
Some representative Hall–petch scaling laws reported in the literature ($\sigma_y=\sigma_0+K_yD^{-1/2}$, where σ_y is the yield point, σ_0 the friction stress, K_y the H–P slope, and D the average grain size).

Material specifications	σ_0 (MPa)	K_y (MPa $m^{1/2}$)	Reference	Note
Grade 2	182	0.36	[27]	Nanostructured
Grade 2	–	0.37	[26]	Microsized
99.998%	–	0.671	[24]	Microsized
99.998%		0.53	[25]	Microsized
Ball-milled	747	0.63	[21]	Nanocrystalline
With O_2, 0°C	186	0.64	[23]	–
Grade 2	163	0.25	Our work	UFG and nanocrystalline

value—a trend that is also seen in FCC metals [28]. Due to the difficulty of synthesizing truly NC Ti with $D < 100$ nm, unfortunately, the H–P slope of Ti has not been extended into the very small D range. Future studies are clearly desirable in order to extend the strength scaling law of Ti down to 15–20 nm.

3.3. Strain rate sensitivity and activation volume

The measured strain rate sensitivity m shown in Fig. 3(c) indicate that it generally increases with the increasing D for UFG-Ti, which at least holds true within the D range (~150–450 nm) we have investigated. This trend reverses the behavior seen in FCC materials; but agrees with m trend observed in another HCP metal Co [11,28]. The calculated activation volume V, on the other hand, does not exhibit a monolithic trend vs. D. This observation is, however, not surprising as the dislocation or twin density has significant effect on V; these quantities are expected to be different in the annealed samples (in additional to the D). The rather small V observed in UFG-Ti may be related to the relative high-density dislocations and easy twining behavior of Ti, which limits the average sweeping distance for dislocation slips. In fact, a V value of $\sim 30b^3$ or less is typically reported for CG- or UFG-Ti in the literature [19,29]. That HCP materials have a rather small V is in sharp contrast to those seen in FCC materials, where V typically varies by 2–3 orders of magnitude (see, for example, Ref. [16]).

3.4. Internal friction measurements and implications

To further understand the deformation mechanisms of UFG-Ti, especially the 350 °C annealed sample, we carried out the internal frictions (IF) measurements. Fig. 4 compares the IF (Q^{-1}) of different samples at a measuring frequency f=0.2 Hz down to the temperature of −150 °C. The ECAP-Ti shows a peak (marked as P_2) at ~ −125 °C, the position of which is consistent with the Hasiguti peak [30] in the range of −150– −73 °C observed in cold-worked CP-Ti and is ascribed to the relaxation of dislocations of the $1/3<11\bar{2}0>/(0001)$ basal slip system at the interstitial sites [31]. Such mechanism was found to have an activation energy far below 0.5 eV [30]. After the UFG-Ti is annealed at 350 °C for 6 h, the peak is weakened which is indicated as a change of slope in the IF near −100 °C. When the annealed UFG-Ti sample is further deformed to ~2% plastic strain, a significant IF peak (marked as P_t) at ~ −70 °C is evident. Interestingly, plastic deformation of the same sample to a larger strain (~6%) does not affect the height and position of the P_t peak. As Hasiguti peak characteristically increases with the increasing plastic strains, it is speculated that the P_t peak around −70 °C is unlikely related to dislocation relaxations.

Fig. 5(a) shows the IF and storage modulus of the ECAP-Ti. The Hasiguti-type P_2 peak is found to be a typical relaxation IF peak accompanied by very little modulus change. Fig. 5(b) compares the IF and storage modulus of the annealed UFG-Ti subjected to 2% strain, manifesting a significant modulus discontinuity close to the peak temperature of the IF P_t peak. Using an Arrhenius relation, the activation energy of these peaks can be calculated based on the frequency-dependent temperatures of the IF peaks obtained by subtracting the backgrounds. The inset of Fig. 4 shows the relation between the measuring frequency f and the peak temperature of peaks P_2 in the ECAP-Ti, and P_t in the annealed UFG-Ti subjected to 2% strains, respectively. The Arrhenius fitting yields activation energies of 0.76 ± 0.05 eV and 0.35 ± 0.04 eV for P_t and P_2 peaks, respectively. The significant differences of the peak temperature and activation energy between P_t and P_2 peaks favor our earlier hypothesis that the P_t peak in the annealed UFG-Ti subjected to 2%–6% strain is not related to the dislocation relaxation. Instead, such large activation energy is typical for the activation of twining dislocations or the relaxation of twin boundary microstructures [24].

4. Conclusions

CP-Ti has been processed into UFG states using ECAP route B_C at room temperature, and excellent tensile properties have been achieved in UFG-Ti, due mainly to the recovery of strain hardening capability despite their submicron grain sizes. The strain rate

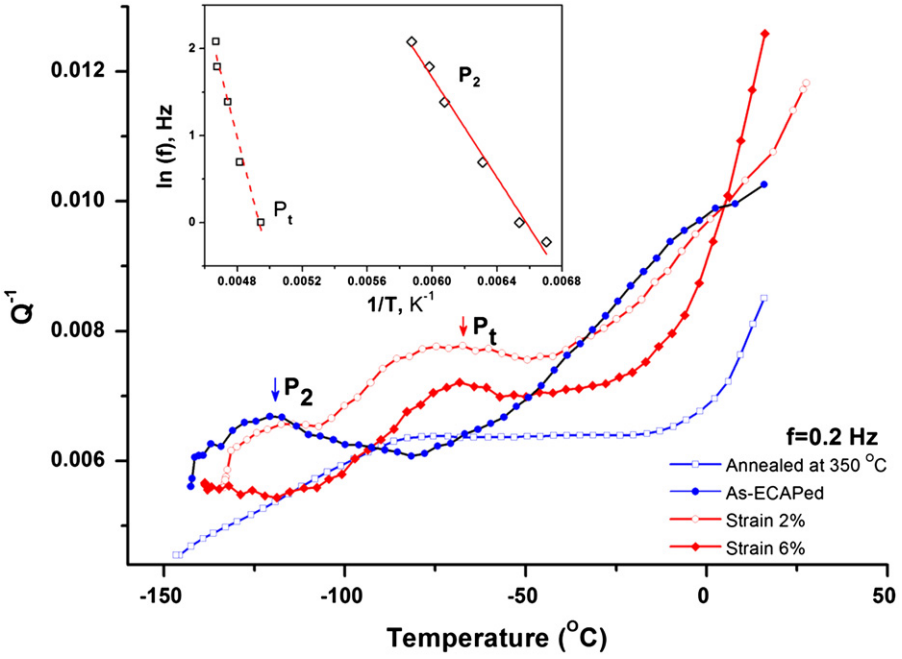

Fig. 4. Internal frictions of the ECAP-Ti, ECAP-Ti annealed at 350 °C for 6 h, deformed (strains 2% and 6%) UFG-Ti annealed at 350 °C for 6 h. The inset is the Arrhenius fits of the P_2 and P_t peaks.

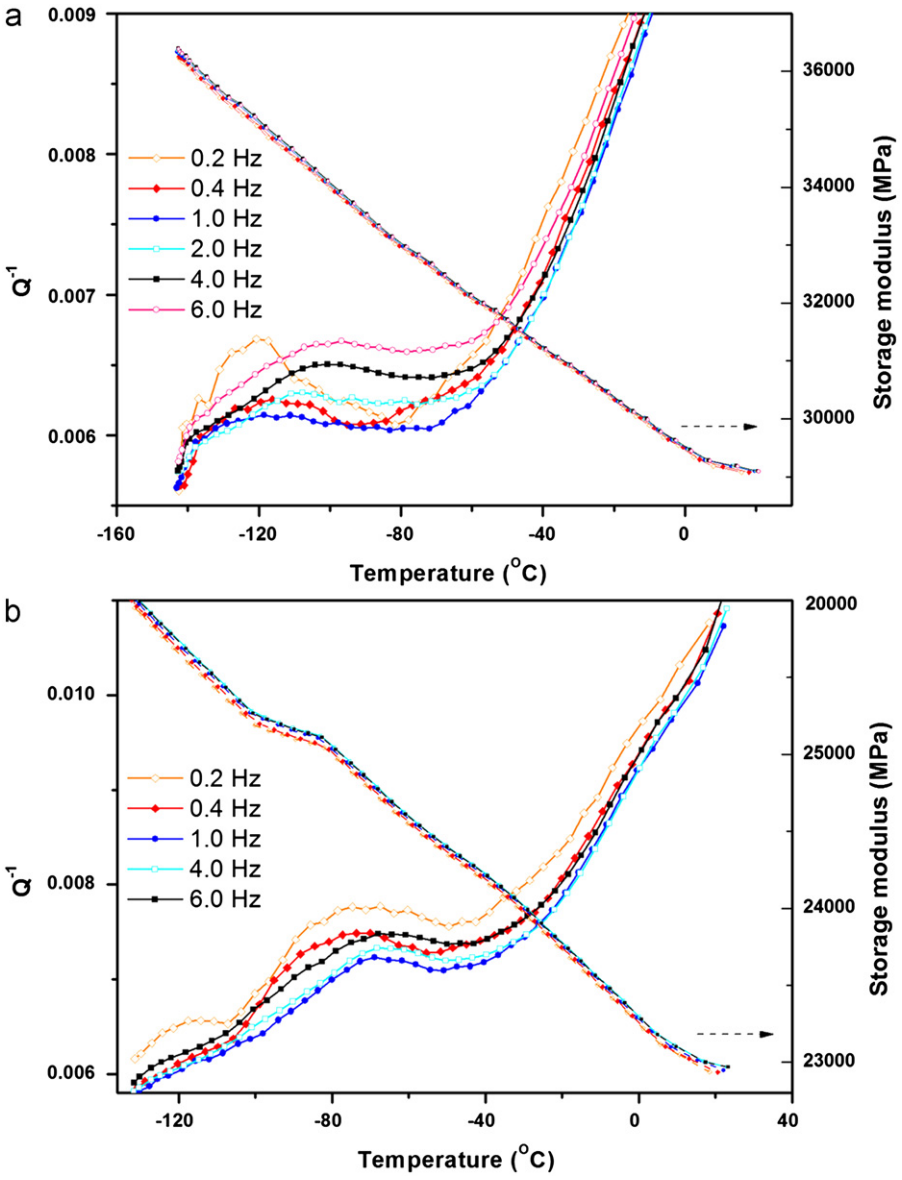

Fig. 5. (a) The IF and storage modulus of the ECAP-Ti at various frequencies. (b) The IF and storage modulus of the annealed UFG-Ti after 2% straining at various frequencies.

sensitivity of HCP Ti is found to decrease with decreasing grain size (~150–450 nm), and the activation volume remains small for all grain sizes, suggestive of the significant roles of twins in these materials. A new H–P scaling law is presented and compared favorably to the literature data. The internal friction analyses suggest that the IF relaxation peak in the 350 °C-annealed UFG-Ti could be related to the twin boundary relaxation. The mechanical testing and internal friction analyses shed some light on the deformation mechanisms of UFG-Ti processed through ECAP, providing useful information on how to develop Ti with high mechanical strength and useful ductility.

Acknowledgment

YKL, FL, and DP gratefully acknowledge the financial support from Shanghai Project no. 10540500900. YKL and GPZ thanks for the supports provided by the Science and Technology Innovation Commission of Shenzhen, China. YHZ is supported by NSFC (no. 51225102), New Century Excellent Talent of Education Department of China, the Fundamental Research Funds for the Central Universities (No. NUST2012ZDJH008), the 8th "Liuda Rencai Gaofeng" of Jiansu Province (no. 2011-XCL-016B), and Gaocengci Chuangxin Chuangye of Jiansu Province. Profs. Valiev and Lavernia are gratefully acknowledged for providing the samples. The work at LLNL was performed under the auspices of the U.S. Department of Energy under Contract no. DE-AC52-07NA27344.

References

[1] R. Valiev, Nat. Mater. 3 (2004) 511–516.
[2] X.C. Zhao, W.J. Fu, X.R. Yang, T.G. Langdon, Scr. Mater. 59 (2008) 542–545.
[3] K.Y. Zhu, A. Vassel, F. Brisset, K. Lu, J. Lu, Acta Mater. 52 (2004) 4101–4110.
[4] D. Jia, Y.M. Wang, K.T. Ramesh, E. Ma, Y.T. Zhu, R.Z. Valiev, Appl. Phys. Lett. 79 (2001) 611–613.
[5] A.V. Sergueeva, V.V. Stolyarov, R.Z. Valiev, A.K. Mukherjee, Scr. Mater. 45 (2001) 747–752.
[6] R.Z. Valiev, A.V. Sergueeva, A.K. Mukherjee, Scr. Mater. 49 (2003) 669–674.
[7] X.L. Wu, N.R. Tao, Q.M. Wei, P. Jiang, J. Lu, K. Lu, Acta Mater. 55 (2007) 5768–5779.

[8] M.R. Barnett, Mater. Sci. Eng. A 464 (2007) 1–7.
[9] Y.T. Zhu, J.Y. Huang, J. Gubicza, T. Ungar, Y.M. Wang, E. Ma, R.Z. Valiev, J. Mater. Res. 18 (2003) 1908–1917.
[10] Q. Yu, Z.W. Shan, J. Li, X.X. Huang, L. Xiao, J. Sun, E. Ma, Nature 463 (2010) 335–338.
[11] Y.M. Wang, R.T. Ott, A.V. Hamza, M.F. Besser, J. Almer, M.J. Kramer, Phys. Rev. Lett. 105 (2010) 215502.
[12] Y.M. Wang, J.Y. Huang, T. Jiao, Y.T. Zhu, A.V. Hamza, J. Mater. Sci. 42 (2007) 1751–1756.
[13] Y.M. Wang, M.W. Chen, F.H. Zhou, E. Ma, Nature 419 (2002) 912–915.
[14] Y.H. Zhao, J.E. Bingert, X.Z. Liao, B.Z. Cui, K. Han, A.V. Sergueeva, A.K. Mukherjee, R.Z. Valiev, T.G. Langdon, Y.T.T. Zhu, Adv. Mater. 18 (2006) 2949–2953.
[15] Y.H. Zhao, T. Topping, J.F. Bingert, J.J. Thornton, A.M. Dangelewicz, Y. Li, W. Liu, Y.T. Zhu, Y.Z. Zhou, E.L. Lavernia, Adv. Mater. 20 (2008) 3028–3033.
[16] J.C. Ye, Y.M. Wang, T.W. Barbee, A.V. Hamza, Appl. Phys. Lett. 100 (2012) 261912.
[17] O. Ertorer, T. Topping, Y. Li, W. Moss, E.J. Lavernia, Scr. Mater. 60 (2009) 586–589.
[18] A.A. Popov, I.Y. Pyshmintsev, S.L. Demakov, A.G. Illarionov, T.C. Lowe, A.V. Sergeyeva, R.Z. Valiev, Scr. Mater. 37 (1997) 1089–1094.
[19] L.S. Fomenko, A.V. Rusakova, S.V. Lubenets, V.A. Moskalenko, Low Temp. Phys. 36 (2010) 645–652.
[20] V.V. Stolyarov, Y.T. Zhu, I.V. Alexandrov, T.C. Lowe, R.Z. Valiev, Mater. Sci. Eng. A 299 (2001) 59–67.
[21] K.Y. Wang, T.D. Shen, M.X. Quan, W.D. Wei, J. Mater. Sci. Lett. 12 (1993) 1818–1820.
[22] V.V. Stolyarov, Y.T. Zhu, I.V. Alexandrov, T.C. Lowe, R.Z. Valiev, Mater. Sci. Eng. A 343 (2003) 43–50.
[23] M.A. Meyers, K.K. Chawla, Mechanical Metallurgy: Principles and Applications, Prentice-Hall, Inc., Englewood Cliffs, New Jersey, 1984.
[24] A.A. Salem, S.R. Kalidindi, R.D. Doherty, Scr. Mater. 46 (2002) 419–423.
[25] A.A. Salem, S.R. Kalidindi, R.D. Doherty, S.L. Semiatin, Metall. Mater. Trans. 37A (2006) 259–268.
[26] N. Stanford, U. Carlson, M.R. Barnett, Metall. Mater. Trans. 39A (2008) 934–944.
[27] P. Luo, D.T. McDonald, W. Xu, S. Palanisamy, M.S. Dargusch, K. Xia, Scr. Mater. 66 (2012) 785–788.
[28] Y.M. Wang, R.T. Ott, T. van Buuren, T.M. Willey, M.M. Biener, A.V. Hamza, Phys. Rev. B 85 (2012) 014101.
[29] V.V. Shpeizman, V.I. Nikolaev, N.N. Peschanskaya, A.E. Romanov, B.I. Smirnov, I.A. Aleksandrov, N.A. Enikeev, V.U. Kazykhanov, A.A. Nazarov, Phys. Solid State 49 (2007) 678–683.
[30] R.R. Hasiguti, G. Kamoshit., N. Igata, Acta Metall. 10 (1962) 442–447.
[31] H. Numakura, Y. Minonishi, M. Koiwa, Philos. Mag. 63 (1991) 785–792.